

Ambiguities in fits of observed binary lens galactic microlensing events

M. Dominik*

Institut für Physik, Universität Dortmund, D-44221 Dortmund, Germany

Received ; accepted

Abstract. For observed galactic microlensing events only one fit is usually presented, though, especially for a binary lens, several fits may be possible. This has been shown for the MACHO LMC#1 event (Dominik & Hirshfeld 1996). Here I discuss the strong binary lens events OGLE#7 and DUO#2. It is shown that several models with a large variety of parameters are in accordance with the photometric data. For most of the fits, $1\text{-}\sigma$ -bounds on the fit parameters are given. The variation of the parameters within these bounds is in some cases considerable. It is likely that other binary lens events which will occur will have properties similar to the discussed events.

Key words: gravitational lensing — dark matter — binaries: general — Stars: low-mass, brown dwarfs — planetary systems

1. Introduction

Some of the observed galactic microlensing events show a signature of a binary lens. The first such event discovered was MACHO LMC#1, where its binary nature has been discussed by Dominik & Hirshfeld (1994, 1996) and by Rhie (1994) and Rhie & Bennett (1996). An explanation with a binary lens has also been proposed for OGLE#6 by Mao & Di Stefano (1995). Neither of these events involves crossings of the source trajectory with the caustics, which would result in sharp spikes¹ in the light curves, which are a clear characteristic of a binary (or multiple) lens. For this reason, these events are called weak binary lens events (according to Mao & Paczyński (1991)). In contrast, the events OGLE#7 (Udalski et al. 1994), DUO#2 (Alard et al. 1995), and MACHO LMC#9 (Bennett et al. 1996) involve such caustic crossings, and are therefore called strong binary lens events. The MACHO collaboration claims at least 5 additional binary lens events in their data obtained with the alert system, namely 95-BLG-12, 96-BLG-3, 97-BLG-1, 97-BLG-28, and 97-BLG-41 (Stubbs et al. 1997). Additional data for these events have been obtained by the MACHO collaboration for the OGLE#7 event (Bennett et al. 1994, 1995; Al-

cock et al. 1997b) and by the PLANET collaboration for the events 95-BLG-12, 97-BLG-28, and 97-BLG-41 (Albrow et al. 1998a,b).

It is a general feature that ambiguities may occur if the data has poor quality, where poor quality means a bad sampling rate and an insufficient photometric accuracy. However, except for the discussion of the MACHO LMC#1 event (Dominik & Hirshfeld 1996), only one model has been presented for the binary lens microlensing events. In this paper, it is shown that several binary lens models can fit the observed data for the events OGLE#7 and DUO#2 showing that these possible ambiguities exist among the observed events. To draw the right conclusions from the observed data it is necessary to find all models which fit the data. Therefore it is interesting to see which types of configurations produce which types of light curves. For the MACHO LMC#1 event, 6 different configurations have been found which can produce an asymmetric light curve of the desired form, so that whenever an event of this form occurs, one should check for (at least) this 6 configurations. In fact, light curves of the type BL and of the type BA can differ by less than 0.3% which is much less than the photometric accuracy actually achieved by the observing teams, so that this ambiguity remains even with a perfect sampling of the data. The arising ambiguities for binary lens events have also been addressed in a recent paper by Di Stefano & Perna (1997).

In this paper, configurations are shown which produce a double caustic crossing (OGLE#7) and a double caustic crossing with a following peak (DUO#2). Though this paper deals with specific events, the types of light curves discussed here are expected to appear more frequently in the data. The configurations shown should be checked as possible solutions for the fit whenever an event of this type occurs. Therefore, this analysis for specific events is instructive in general, even if additional observations show that some of the models can be ruled out for these specific events. Better than what can be done by a simulation, the observed events show the actual quality of the data.

To extract the underlying physical quantities like the masses of the lens objects, it is of interest to see how well the observed data constrains the fit parameters. Except for MACHO LMC#1 (Dominik & Hirshfeld 1994, 1996), no error bounds on the fit parameters have been given for binary lens

* *Present address:* Kapteyn Instituut, Rijksuniversiteit Groningen, Postbus 800, NL-9700 AV Groningen, The Netherlands (dominik@astro.rug.nl)

¹ or at least a dramatic rise and fall for larger sources

events. In this paper, these error bounds are given for most of the fits for OGLE#7 and DUO#2.

Section 2 reviews the basics of galactic microlensing with binary lenses, Sect. 3 gives the discussion of the OGLE#7 event, while the DUO#2 event is discussed in Sect. 4. In Sect. 5 the results are summarized.

2. Galactic microlensing with binary lenses

Consider a lens at a distance D_d from the observer, a source at a distance D_s from the observer, and let D_{ds} be the lens-source distance. The Einstein radius for a lens of mass M is then given by

$$r_E = \sqrt{\frac{4GM}{c^2} \frac{D_d D_{ds}}{D_s}}. \quad (1)$$

Further consider an optical axis through observer and lens center and planes perpendicular to it at the position of the lens (lens plane) and the source (source plane) centered at the optical axis. Let the source be located at $\boldsymbol{\eta} = \frac{D_s}{D_d} r_E \mathbf{y}$ in the source plane and let a light ray pass from the source to the observer through the lens plane at $\boldsymbol{\xi} = r_E \mathbf{x}$.

For a binary lens consisting of a mass with fraction m_1 of the total mass M at $(r_{hd}, 0)$ and a mass with fraction $m_2 = 1 - m_1$ at $(-r_{hd}, 0)$, where $r_{hd} = \chi r_E$, the coordinates \mathbf{x} and \mathbf{y} are related by the lens equation

$$y_1(x_1, x_2) = x_1 - m_1 \frac{x_1 - \chi}{(x_1 - \chi)^2 + x_2^2} - (1 - m_1) \frac{x_1 + \chi}{(x_1 + \chi)^2 + x_2^2}, \quad (2)$$

$$y_2(x_1, x_2) = x_2 - m_1 \frac{x_2}{(x_1 - \chi)^2 + x_2^2} - (1 - m_1) \frac{x_2}{(x_1 + \chi)^2 + x_2^2}, \quad (3)$$

which gives the true source position as a function of the observed image position. For a given source position, there are either 3 or 5 images. To obtain the images for a given source position \mathbf{y} one has to solve the lens equation numerically.

The magnification μ of an image at \mathbf{x} is given by the inverse of the Jacobian determinant of the mapping, i.e.

$$\mu(\mathbf{x}) = \frac{1}{\left| \det \left(\frac{\partial \mathbf{y}}{\partial \mathbf{x}} \right) \right|}, \quad (4)$$

and the total magnification of a (point) source $\tilde{\mu}(\mathbf{y})$ is given as the sum of the magnifications of the individual images. A (point) source is located on a caustic if $\mu(\mathbf{x})$ diverges for at least one image \mathbf{x} . The magnification of an extended source is obtained by integrating over the point source magnifications.

Let the source move on a straight line with a velocity v_\perp projected onto the lens plane transverse to the line-of-sight between observer and lens, so that it moves one Einstein radius in the lens plane in the time $t_E = \frac{r_E}{v_\perp}$.² For the fits, a timescale

² Note that this is equivalent to letting the lens move with v_\perp into the opposite direction. Further note that if the fixed source is on the

$t_c = 2t_E$ is used. In addition, the following parameters are used (see Fig. 1)³: The source trajectory projected to the lens plane has the closest approach to the origin at the time t_{\max} and the distance $r_{\min} = u_{\min} r_E$. The angle α is measured between the x_1 -direction and the direction of motion of the source. To get uniqueness in parameter space, the sign of the velocity of the source is chosen so that the midpoint of the lens system is on the right hand side of the line traced in time by the source and the parameter ranges are $u_{\min} \geq 0$, $0 \leq \alpha < \pi$ and $0 \leq m_1 \leq 1$.

The observed amplification of the source object as a function of time $A(t)$ has been calculated efficiently by solving the lens equation for the whole source trajectory simultaneously (Dominik 1995) and by determining the magnification from the images with Eq. (4).

Fig. 1. The geometry of a binary lens event

Another parametrization for binary lenses has been used by Mao & Di Stefano (1995). The main difference is that they refer the closest approach of the source to the center of mass of the lens system and not to the midpoint. The translation between the parameter sets is shown in Table 1.

The amount of additional light contributed by other objects than the 'source' is described by the blending parameter f . It gives the contribution of the light of the unlensed source to the total light. If $A(t)$ denotes the amplification of the source, the observed amplification is given by

$$A_{\text{tot}} = fA(t) + 1 - f. \quad (5)$$

3. An event with two caustic crossings: OGLE #7

The OGLE#7 event (Udalski et al. 1994, hereafter USM) is the first event observed which shows the signature of a strong binary lens. In contrast to the MACHO LMC#1 event, it is clear that a single lens cannot explain the data, because it will produce neither spikes nor a plateau formed like a U, irrespective of whether the source is a binary or not or whether the objects

right side of the lens trajectory, a corresponding fixed lens is on the right side of the source trajectory.

³ These parameters coincide with those which have been used in (Dominik & Hirshfeld 1994, 1996)

Table 1. The translation between different parameter sets for binary lens models

Mao & Di Stefano → Dominik	Dominik → Mao & Di Stefano
$\alpha[\text{rad}] = \frac{\pi}{180}\vartheta[^\circ]$	$\vartheta[^\circ] = \frac{180}{\pi}\alpha[\text{rad}]$
$m_1 = \frac{q}{q+1}$	$q = \frac{m_1}{1-m_1}$
$\chi = a/2$	$a = 2\chi$
$t_c = 2t_E$	$t_E = t_c/2$
$r_{\min} = b - \frac{a}{2} \frac{q-1}{q+1} \sin \vartheta$	$b = r_{\min} - \chi(1-2m_1) \sin \alpha$
$t_{\max} = t_b - \frac{a}{2} \frac{q-1}{q+1} t_E \cos \vartheta$	$t_b = t_{\max} - \chi(1-2m_1) \frac{t_c}{2} \cos \alpha$

are extended. A first fit to the data has been presented in USM. However, several binary lens fits for these data are possible. In Tables 2 and 3, I present the results of 8 different fits. The χ^2 corresponds to the original errors given by the OGLE collaboration. The errors on the parameters correspond to projections of the hypersurface $\Delta\chi^2 = \chi^2 - \chi_{\min}^2 = 1$ onto the axes in parameter space. The characteristic time ranges from 162 d (BL0) to 1470 d (BL6) which means that the expected total mass ($\propto t_c^2$) varies by a factor of 80. The mass ratio ranges from about 1 (BL0, BL6, BL7) to 16 (BL). The contribution of external light (blending) at the minimum light ranges from 17 % (BL9) to 94 % (BL). Note that some of the errors on t_c are large: For BL2 the 1- σ error is about 25 % of the value, for BL7, BL1, BL3, and BL9 the 1- σ errors are also about 10–20 % of the value of t_c . The second pair of caustic crossings for the BL-fit and the caustic crossings on the triangle shaped caustic for the BL6-fit posed additional problems for the calculation of the error bounds, so that no error bounds are shown for these fits.

The fit of USM corresponds to the BL0-fit. Table 4 shows the parameters of the BL0-fit in the parametrization used in USM and the parameters quoted there. Note that their m_0 is the magnitude of the lensed component, while m_{base} corresponds to the minimum light observed, i.e. the light from the lensed and the unlensed component. These quantities are therefore related by

$$m_0 = -m_{\text{base}} - 2.5 \lg f. \quad (6)$$

If one accepts the given error bars of the data points, one sees that the values of χ_{\min}^2 are very bad (see Table 5). If one adapts the size of the error bars to the tail data points in the same way as for the MACHO LMC#1 event (Dominik & Hirschfeld 1996), but with Gaussian errors⁴, defining all data points for $t < 900$ d as belonging to the 'tail', one obtains a scaling factor of $\gamma = 1.597$, which means that the errors are enlarged by about 60 %. The probabilities for the fits become ≥ 84 %

⁴ As shown for the MACHO LMC#1 event (Dominik 1996) the results do not differ much if one uses a larger rescaling factor with a distribution with smaller tail or a smaller rescaling factor with a distribution with larger tail. Since there are only a few data points in the tail region (32), the extraction of non-Gaussian behaviour is not successful (Dominik 1996).

Table 4. OGLE #7: The BL0-fit and the fit of USM

parameter	BL0	Udalski et al.
t_E [d]	80.88	80
t_b [d]	1172.89	1172.5
a	1.1309	1.14
q	1.024	1.02
θ [°]	131.68	138.3
b	0.0532	0.050
m_0	18.152	18.1
f	0.5573	0.56

for all fits and ≥ 95 % for all fits except for BL3 and BL9. If one looks carefully at the light curve and the data, one sees that the data point in the tail at $t = 806.60603$ and $I = 17.794$ contributes about 33 to the total χ^2 . If one omits this discrepant point, one gets a rescaling factor of $\gamma = 1.247$ and the results shown in Table 6. If one assumes that the discrepant point in the tail is due to a measurement error, and taking into account that the error bars may be about 15–25 % too small, one can accept all 8 models (see Table 6). If one does not ascribe the discrepant point to a measurement error, one has to accept the large rescaling factor to allow the tail to be constant. Also in this case, all the fits are acceptable. Note that the errors may show some non-Gaussian behaviour. This behaviour is effectively absorbed into the rescaling factor in my analysis.

The light curves for the fits are shown in Fig. 2 and the structure of the caustics together with the source trajectory can be seen in Fig. 3. The distance scale used is projected Einstein radii ($r'_E = \frac{D_s}{D_d} r_E$) of the total mass in the source plane. The intersections of the source trajectory with the caustics and the projected positions of the lens objects are indicated by small crosses. The tip of the arrow on the trajectory denotes the closest approach to the coordinate origin.

Additional data for this event has been obtained by the MACHO collaboration (Bennett et al. 1994, 1995; Alcock et al. 1997b). The main feature of this data is a data point (in two bands) on the fall of the second caustic crossing, which can only be fitted by including a finite source size. If one omits

Table 2. OGLE #7: Fits for a strong binary lens event

parameter	BL2	BL0	BL1	BL7
t_c [d]	345_{-82}^{+95}	$161.8_{-6.9}^{+6.8}$	291_{-19}^{+41}	350_{-39}^{+52}
t_{\max} [d]	$1147.6_{-7.4}^{+4.7}$	$1173.3_{-2.0}^{+2.5}$	$1164.6_{-1.5}^{+1.2}$	$1150.86_{-10.5}^{+0.47}$
χ	$0.400_{-0.028}^{+0.041}$	$0.565_{-0.010}^{+0.011}$	$0.387_{-0.013}^{+0.030}$	$0.496_{-0.011}^{+0.021}$
m_1	$0.268_{-0.054}^{+0.082}$	$0.506_{-0.014}^{+0.029}$	$0.397_{-0.015}^{+0.089}$	$0.518_{-0.043}^{+0.022}$
α [rad]	$2.517_{-0.062}^{+0.028}$	$2.297_{-0.048}^{+0.044}$	$1.635_{-0.026}^{+0.025}$	$0.135_{-0.099}^{+0.025}$
u_{\min}	$0.013_{-0.012}^{+0.006}$	$0.048_{-0.006}^{+0.013}$	$0.01100_{-0.020}^{+0.00088}$	$0.539_{-0.060}^{+0.054}$
m_{base}	$-17.5299_{-0.0077}^{+0.0079}$	$-17.5171_{-0.0070}^{+0.0071}$	$-17.5260_{-0.0088}^{+0.0077}$	$-17.5487_{-0.013}^{+0.0091}$
f	$0.241_{-0.041}^{+0.066}$	$0.557_{-0.022}^{+0.020}$	$0.243_{-0.014}^{+0.017}$	$0.618_{-0.019}^{+0.019}$
χ_{\min}^2	133.94	137.73	137.93	140.25

Table 3. OGLE #7: Fits for a strong binary lens event

parameter	BL6	BL	BL3	BL9
t_c [d]	1470.84	1299.68	440.56_{-26}^{+43}	495_{-70}^{+73}
t_{\max} [d]	2149.92	1380.10	$1168.4_{-2.7}^{+2.1}$	$1160.93_{-2.4}^{+0.95}$
χ	0.2813	0.3725	$0.854_{-0.039}^{+0.044}$	$0.736_{-0.010}^{+0.014}$
m_1	0.510	0.059	$0.759_{-0.11}^{+0.081}$	$0.938_{-0.009}^{+0.024}$
α [rad]	2.050	0.414	$1.567_{-0.025}^{+0.031}$	$1.942_{-0.054}^{+0.043}$
u_{\min}	0.649	0.068	$0.316_{-0.064}^{+0.077}$	$0.086_{-0.023}^{+0.027}$
m_{base}	-17.5868	-17.5555	$-17.5538_{-0.0096}^{+0.0079}$	$-17.639_{-0.030}^{+0.031}$
f	0.667	0.057	$0.578_{-0.064}^{+0.052}$	$0.829_{-0.043}^{+0.032}$
χ_{\min}^2	141.49	143.41	150.95	160.06

Table 5. OGLE #7: χ_{\min}^2 and the corresponding probability without rescaling

	BL2	BL0	BL1	BL7	BL6	BL	BL3	BL9
χ_{\min}^2	133.94	137.73	137.93	140.25	141.49	143.41	150.95	160.06
$\sqrt{2\chi_{\min}^2 - \sqrt{2n-1}}$	4.160	4.390	4.402	4.542	4.615	4.729	5.169	5.685
$P(\chi^2 \geq \chi_{\min}^2)$	$2 \cdot 10^{-5}$	$6 \cdot 10^{-6}$	$5 \cdot 10^{-6}$	$3 \cdot 10^{-6}$	$2 \cdot 10^{-6}$	$1 \cdot 10^{-6}$	$1 \cdot 10^{-7}$	$7 \cdot 10^{-9}$

this point, models with configurations similar to BL7, BL2, BL1, BL3, and BL0 give good fits (in descending order),⁵ BL is marginal and BL6 and BL9 are excluded. If one includes the point on the fall of the second caustic crossing, the approximation of a point source fails. If one allows for a finite source size, there are still several possible models remaining, with parameters similar to the above point-source fits: Models similar to BL1, BL0, BL2, and BL3 give successful fits (in descending order of goodness-of-fit). The additional MACHO

⁵ The MACHO collaboration did not make this data available in electronic form, these statements are based on data obtained by reading off the values from their figures.

data is therefore not sufficient to break the ambiguities for this event completely. Nevertheless, it is advisory to test all of the above types of configurations for an event like OGLE#7 to see whether there are fit ambiguities and to find a suitable model.

4. An event with two caustic crossings and an additional peak: DUO #2

The DUO#2 event has been reported by Alard et al. (1995), hereafter AMG, where a fit with a strong binary lens is presented. The corresponding fit parameters using my parameter set are shown in Table 7. For 116 data points, a χ^2 of 89 is

Table 6. OGLE #7: χ^2_{\min} and the corresponding probability without discrepant point with rescaling

	BL2	BL0	BL1	BL7	BL6	BL	BL3	BL9
χ^2_{\min}	64.98	66.92	67.55	68.65	69.71	70.37	76.60	80.86
$\sqrt{2\chi^2_{\min}} - \sqrt{2n-1}$	-0.807	-0.638	-0.583	-0.489	-0.399	-0.343	0.171	0.510
$P(\chi^2 \geq \chi^2_{\min})$	79 %	74 %	72 %	69 %	66 %	63 %	43 %	30 %

reached, where the source is treated as extended ($R_{\text{src}} \lesssim 10^{-2}$) and limb-darkened with $\tilde{u}_{\text{blue}} = 0.6$ and $\tilde{u}_{\text{red}} = 0.5$, where the brightness profile of the source is of the form

$$f(r, \tilde{u}) = \tilde{u}\sqrt{1-r^2} + 1 - \tilde{u}, \quad (7)$$

r being the ratio of the actual radius and the total radius.

Here I show additional possible fits using a static binary lens and a point source. I have omitted one occurrence of a data point which appeared twice in the data I have received from C. Alard, so that I use 115 data points and not 116 data points as in AMG. Moreover, I use the magnitude values for the fit and not the amplification values as used for the fit in AMG (S. Mao, private communication). From this, only a small difference results (Dominik 1996), the χ^2_{\min} differs only by about 2 units and the fit parameters show only small differences which are well within the bounds corresponding to $\Delta\chi^2 = 1$. The analysis of the tail data points ($t < 70$ d or $t > 100$ d) yielded most-likely scaling factors $\gamma_{\text{blue}} = 0.912$ for 63 data points and $\gamma_{\text{red}} = 0.828$ for 25 data points. These values are close to 1 (note that there are only a few tail data points), so that the tail seems to be consistent with a constant brightness and no further scaling is used in this discussion. The results of the fits are shown in Tables 8 and 9. The quoted error bounds correspond to projections of the hypersurface $\Delta\chi^2 = 1$ onto the axes in parameter space. An asterisk (*) denotes that the numerical routines have ended up at a jump discontinuity. It is not yet clear if this is a real effect or if it is due to difficulties in the computation. There appear additional minima, whose $\Delta\chi^2 \leq 1$ -regions include other minima with smaller χ^2 . In particular, this is a problem for the BL1-, BL2-, and the BL4-fit which also makes the calculation of the error bounds difficult, so that they are not shown in the tables for these fits. This behavior is influenced by the fact that there are only a few data points to constrain the shape of the light curve in the peak region.

One sees that the BL- and the BL4-fit give good explanations of the observed data, while the BL2-, BL3-, and the BL5-fit give worse results, although they are not totally excluded. The BL1-fit gives such a low probability that it is excluded. Light curves of the peak region ($70 \text{ d} \leq t \leq 100 \text{ d}$) for both spectral bands together with the data points are shown in Figs. 4 and 5, where the upper curve refers to the blue band and the lower curve refers to the red band. Note that the largest differences between the BL-fit and the extended source fit near the BL-parameters occur in the peak after the caustic crossings, not in the caustic crossings themselves.

Fig. 6. DUO #2: Light curves for the fit near BL with an extended source and the measured data points. Light curve for the blue spectral band on the top and light curve for the red spectral band on the bottom.

The configurations for the different models are shown in Fig. 7, where the caustics are shown together with the trajectory of the moving point source. The projected positions of the lens objects and the intersections of the source trajectory with the caustics are indicated by small crosses. All distances are measured in Einstein radii r_E if the projection to the lens plane is considered or in projected Einstein radii r'_E if the projection to the source plane is considered.

Taking into account the error bounds, the BL-fit seems to coincide with the fit in AMG, except for the small lower bound on χ , which however may be relic of computational problems. Near the parameters for the BL-fit, I have started a fit including an extended source. As for the fit of AMG, the source brightness profile has been fixed to a limb-darkening profile with $\tilde{u}_{\text{blue}} = 0.6$ and $\tilde{u}_{\text{red}} = 0.5$. The resulting fit parameters are shown in Table 10. Note that this fit gives only a slightly better χ^2_{\min} than the BL-fit with a point source. The parameters coincide with the BL-fit as well as with the fit of AMG. It is not clear to me how the $\chi^2_{\min} = 89$ of AMG is reached. For their fit parameters (S. Mao, private communication), I obtain a χ^2 which is larger than the χ^2_{\min} for the extended source fit.

Fig. 2. OGLE#7: Light curves for the different binary lens fits and measured data points in I-band. From left to right, top to bottom: (a) BL2, (b) BL0, (c) BL1, (d) BL7, (e) BL6, (f) BL, (g) BL3, (h) BL9.

A peak near a caustic crossing can also be modeled in a different way with a rotating binary lens. With parameters similar to those used for the model BL0 for OGLE#7, a peak after

the caustic crossing can be modeled by including the rotation (Dominik 1998b).

In AMG, it has been addressed that the observation of the position of the blend together with the observation of the shift

Table 8. DUO #2: Fits for a strong binary lens event

parameter	BL	BL4	BL2
t_c [d]	$18.9^{+2.5}_{-1.5}$	23.79	16.40
t_{\max} [d]	$85.234^{+0.075}_{-0.062}$	89.247	88.351
χ	$0.6434^{+0.050}_{-0.0011*}$	0.4058	0.4571
m_1	$0.759^{+0.005}_{-0.026}$	0.176	0.829
α [rad]	$1.496^{+0.023}_{-0.024}$	0.670	2.576
u_{\min}	$0.157^{+0.025*}_{-0.043*}$	0.00684	0.0406
$m_{\text{base,blue}}$	$-20.2077^{+0.0061}_{-0.0059}$	-20.2087	-20.2046
$m_{\text{base,red}}$	$-18.575^{+0.011}_{-0.011}$	-18.5777	-18.5733
f_{blue}	$0.708^{+0.035}_{-0.048}$	0.260	0.418
f_{red}	$0.702^{+0.044}_{-0.054}$	0.266	0.441
χ^2_{\min}	109.45	111.57	131.17
$n = \# \text{ d.o.f.}$	105	105	105
$\sqrt{2\chi^2_{\min} - \sqrt{2n - 1}}$	0.338	0.481	1.740
$P(\chi^2 \geq \chi^2_{\min})$	37 %	32 %	4 %

Table 9. DUO #2: Fits for a strong binary lens event

parameter	BL3	BL5	BL1
t_c [d]	$14.95^{+0.94}_{-0.93}$	$12.30^{+0.21*}_{-0.57}$	14.40
t_{\max} [d]	$85.69^{+0.15}_{-0.24}$	$84.29^{+0.06*}_{-0.28}$	85.99
χ	$0.7832^{+0.0068}_{-0.0078}$	$0.495^{+0.009}_{-0.005*}$	0.649
m_1	$0.263^{+0.036}_{-0.024}$	$0.195^{+0.030}_{-0.031}$	0.394
α [rad]	$0.536^{+0.022}_{-0.030}$	$2.260^{+0.071}_{-0.044*}$	0.423
u_{\min}	$0.053^{+0.011}_{-0.017}$	$0.161^{+0.017}_{-0.016}$	0.261
$m_{\text{base,blue}}$	$-20.2075^{+0.0065}_{-0.0062}$	$-20.1980^{+0.0057}_{-0.0057}$	-20.2059
$m_{\text{base,red}}$	$-18.574^{+0.011}_{-0.011}$	$-18.564^{+0.011}_{-0.011}$	-18.573
f_{blue}	$0.886^{+0.024}_{-0.037*}$	$0.548^{+0.042}_{-0.042}$	0.803
f_{red}	$0.872^{+0.037}_{-0.042}$	$0.529^{+0.044}_{-0.044}$	0.795
χ^2_{\min}	134.96	137.63	168.39
$n = \# \text{ d.o.f.}$	105	105	105
$\sqrt{2\chi^2_{\min} - \sqrt{2n - 1}}$	1.973	2.134	3.89
$P(\chi^2 \geq \chi^2_{\min})$	2 %	2 %	$5 \cdot 10^{-5}$

in the centroid of light gives an additional constraint. In fact, with these observations, a constraint on the blending parameter f is obtained. The observed data for the centroid shift and the position of the blend should rule out the models BL4 and BL2, leaving the model BL (which had been proposed by AMG) as the most likely interpretation, though the BL5 model does not seem to be completely excluded.

5. Summary of results

It has been shown that there are several models which fit the observed photometric data for the strong binary lens events OGLE#7 and DUO#2, as well as for the weak binary lens event MACHO LMC#1 (Dominik & Hirshfeld 1996). A large variety of timescales results, so that the expectation value for the mass (see Dominik 1998a) differs by a factor of 80 for the different fits for OGLE#7. In addition, the uncertainty in t_c for a given fit as given by the 1- σ -bound is as large as 25 %

Table 7. DUO #2: Fit of AMG

parameter	DUO#2 in AMG
t_c [d]	17
t_{\max} [d]	85.19
χ	0.605
m_1	0.752
α [rad]	1.490
u_{\min}	0.096
$m_{\text{base,blue}}$	-20.21
$m_{\text{base,red}}$	-18.55
f_{blue}	0.73
f_{red}	0.70

Table 10. DUO #2: Fit for a strong binary lens and an extended source

parameter	binary lens, extended source
t_c [d]	19.1
t_{\max} [d]	85.18
χ	0.626
m_1	0.738
α [rad]	1.447
u_{\min}	0.159
$m_{\text{base,blue}}$	-20.207
$m_{\text{base,red}}$	-18.575
f_{blue}	0.665
f_{red}	0.657
R_{src}	0.0012
χ_{\min}^2	107.28
$n = \# \text{ d.o.f.}$	104
$\sqrt{2\chi_{\min}^2} - \sqrt{2n-1}$	0.260
$P(\chi^2 \geq \chi_{\min}^2)$	40 %

for OGLE#7, which is substantially larger than for MACHO LMC#1 or events described by single point-mass lenses.

While ambiguities for DUO#2 are due to the bad sampling rate, the light curves for the different models are much more similar for OGLE#7 and MACHO LMC#1, so that even for a good (or perfect) sampling, ambiguities may occur due to the limited photometric precision. Whether there are ambiguities or not for a given photometric precision depends on the distinctive features that are present in the light curve. The asymmetric peak is a less distinctive feature than the double caustic crossing of OGLE#7, an asymmetric peak can also be modeled by a binary source, while the spikes at the caustic crossing clearly indicate a lens binary (or multiple). The additional

peak for DUO#2 is an additional distinctive feature compared to OGLE#7. More distinctive features can be present if one can observe the finite source size (Alcock et al. 1997a; Albrow et al. 1998b), or rotation effects (Dominik 1998b) in the photometric data, where rotation effects can be the earth-sun parallax (Alcock et al. 1997a) the rotation of a binary source (Paczynski 1997) or of a binary lens (example yet to be detected). Some of the ambiguities may also disappear if one can observe blending shifts and identify the blend (Alard et al. 1995) or resolve the motion of the centroid of light due to the motion and brightening of the images (Høg et al. 1995; Paczynski 1998; Boden et al. 1998).

This paper shows that it is of importance to look for all possible fits. The models shown (and by Dominik & Hirshfeld (1996) for MACHO LMC#1) here give some insight to the possible configurations which arise for the presented type of models.

Especially for claiming the existence of a planet from a microlensing light curve, one has to be careful and study all possible models and consider the uncertainties of the fit parameters as given e.g. by 1- σ -bounds (see also Gaudi & Gould 1997; Gaudi 1997). From these fit parameters, information about the physical quantities (mass, separation) can be obtained (Dominik 1998a).

Acknowledgements. I would like to thank S. Mao for some discussions on the subject, C. Alard for sending me the data of the DUO#2 event, the OGLE collaboration for making available their data, and A. C. Hirshfeld for reading the draft manuscript.

References

- Alard C., Mao S., Guibert J., 1995, A&A 300, L17
- Albrow M., Beaulieu J.-P., Birch P., et al. (The PLANET collaboration), 1998a, The 1995 pilot campaign of PLANET: Searching for microlensing anomalies through precise, rapid, round-the-clock monitoring, accepted for publication in ApJ 509
- Albrow M., Beaulieu J.-P., Caldwell J. A. R., et al. (The PLANET collaboration), 1998b, 1997 PLANET monitoring of anomalous events: First detection of limb-darkening via microlensing, Proceedings of the 4th International workshop on gravitational microlensing surveys, eds. J. Kaplan & M. Moniez
- Alcock C., Allen W. H., Allsman R. A., et al. (The MACHO and GMAN collaborations), 1997a, ApJ 491, 436
- Alcock C., Allsman R. A., Alves D., et al. (The MACHO collaboration), 1997, ApJ 479, 119
- Bennett D. P., Alcock C., Allsman R. A., et al. (The MACHO collaboration), 1994, Recent developments in gravitational microlensing and the latest MACHO results: Microlensing towards the galactic bulge, Proceedings of 5th Annual Astrophysics Conference in Maryland, ed. S. Holt, preprint astro-ph/9411114
- Bennett D. P., Alcock C., Allsman R. A., et al. (The MACHO collaboration), 1995, The MACHO project dark matter search, Proceedings of the Astronomical Society of the Pacific Symposium on Clusters, Lensing, and the Future of the Universe, preprint astro-ph/9510104
- Bennett D. P., Alcock C., Allsman R. A., et al. (The MACHO collaboration), 1996, Nucl. Phys. Proc. Suppl. 51B, 152
- Boden A. F., Shao M., Van Buren D., 1998, ApJ 502, 538

- Di Stefano R., Perna R., 1997, ApJ 488, 55
- Dominik M., 1995, A&AS 109, 597
- Dominik M., 1996, Galactic Microlensing beyond the Standard Model, PhD thesis, Universität Dortmund
- Dominik M., 1998a, A&A 329, 361
- Dominik M., 1998b, A&A 330, 963
- Dominik M., Hirshfeld A. C., 1994, A&A 289, L31
- Dominik M., Hirshfeld A. C., 1996, A&A 313, 841
- Gaudi B. S., 1997, Planet microlensing perturbations: True planets or binary source?, preprint astro-ph/9706268
- Gaudi B. S., Gould A., 1997, ApJ 486, 85
- Høg E., Novikov I. D., Polnarev A. G., 1995, A&A 294, 287
- Mao S., Di Stefano R., 1995, ApJ 440, 22
- Mao S., Paczyński B., 1991, ApJ 374, L37
- Paczynski B., 1997, Binary source parallactic effect in gravitational micro-lensing, preprint astro-ph/9711007
- Paczynski B., 1998, ApJ 494, L23
- Rhie S. H., 1994, contributed talk in the conference "Sources of dark matter in the universe", 16-18 February (unpublished)
- Rhie S. H., Bennett D. P., 1996, Nucl. Phys. Proc. Suppl. 51B, 86
- Stubbs C., et al. (MACHO collaboration), 1997, <http://darkstar.astro.washington.edu>
- Udalski A., Szymański M., Mao S., et al., 1994, ApJ 436, L103

Fig. 3. OGLE#7. Caustics and source trajectory for the different binary lens fits. The distance is measured in projected Einstein radii of the total mass. Small crosses indicate crossings of the source trajectory with the caustics and the projected positions of the point masses. From left to right, top to bottom: (a) BL2, (b) BL0, (c) BL1, (d) BL7, (e) BL6, (f) BL, (g) BL3, (h) BL9.

Fig. 4. DUO #2: Light curves for the different binary lens fits and measured data points. Light curve for the blue spectral band on the top and light curve for the red spectral band on the bottom. From left to right, top to bottom: (a) BL, (b) BL4, (c) BL2, (d) BL3.

Fig. 5. DUO #2: Light curves for the different binary lens fits and measured data points. Light curve for the blue spectral band on the top and light curve for the red spectral band on the bottom. From left to right: (a) BL5, (b) BL1.

Fig. 7. DUO #2: Caustics and source trajectory for the different binary lens fits. From left to right, top to bottom: (a) BL, (b) BL4, (c) BL2, (d) BL3, (e) BL5, (f) BL1.

Figure 1

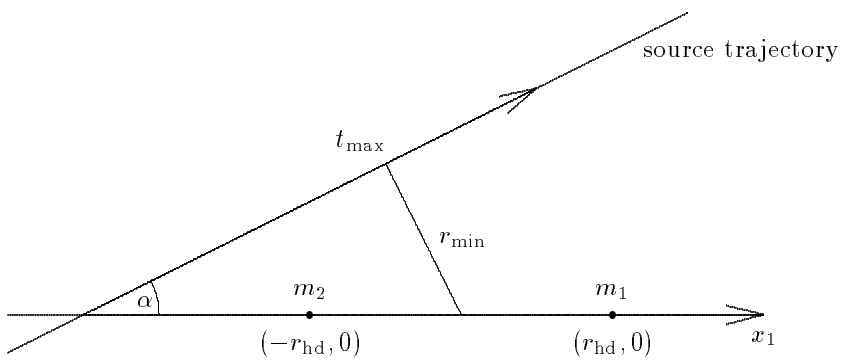


Figure 2a

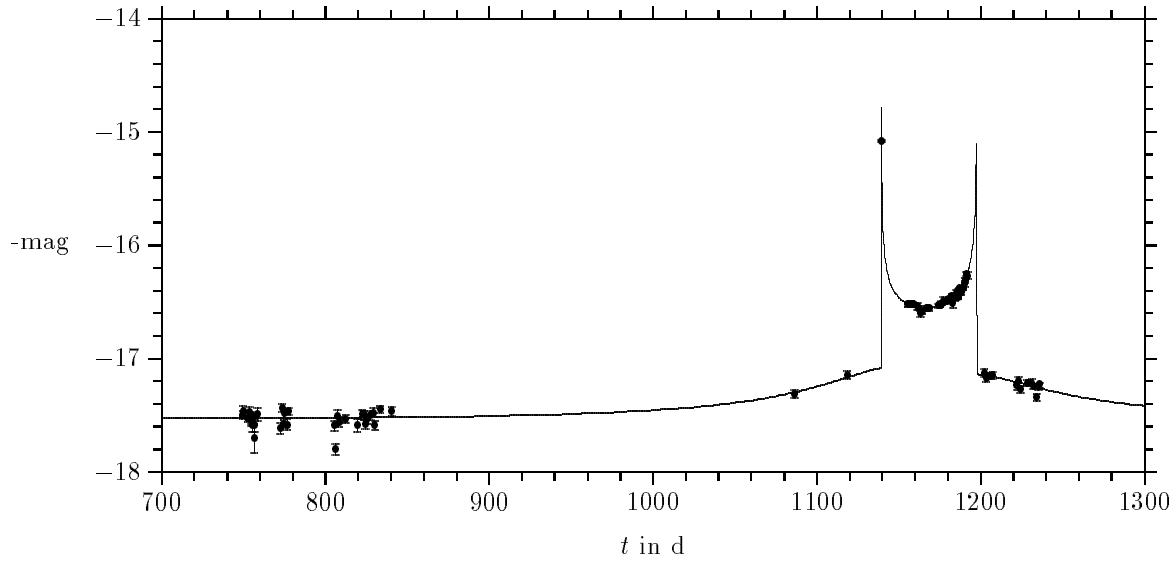


Figure 2b

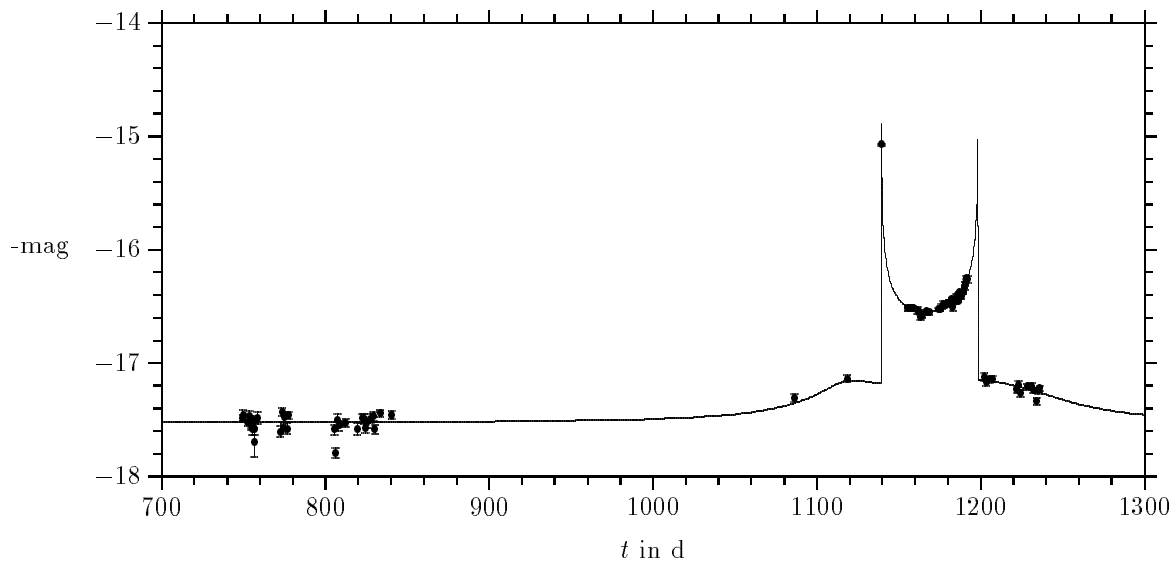


Figure 2c

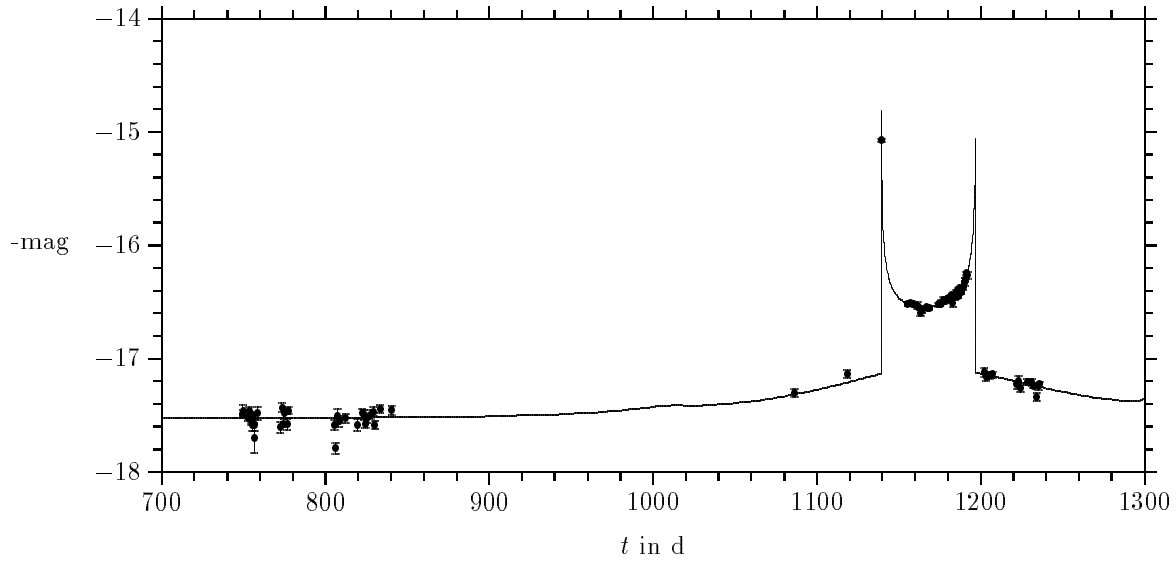


Figure 2d

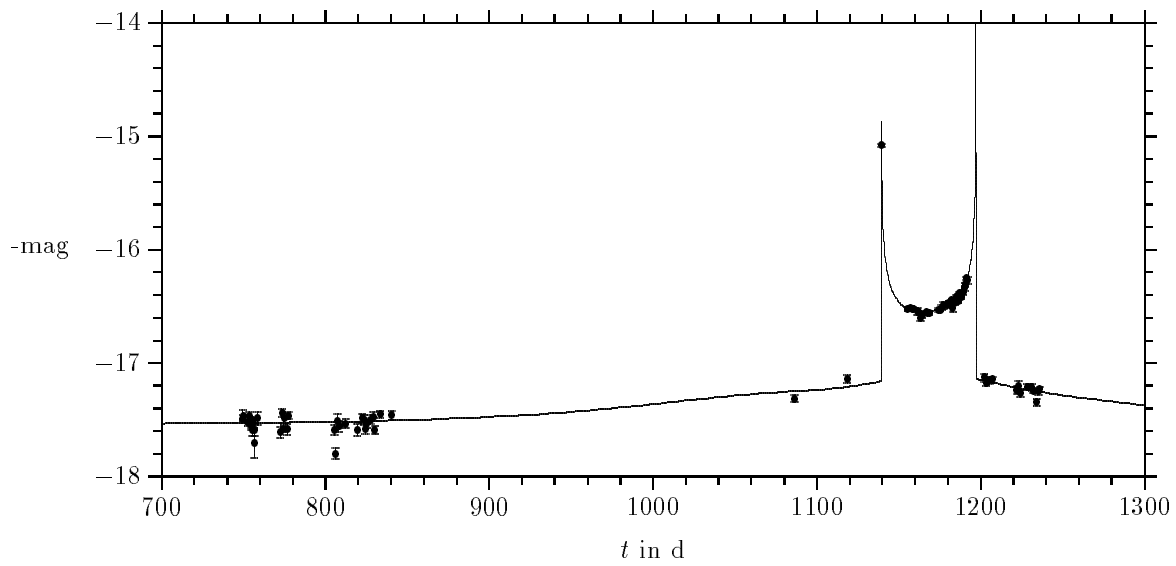


Figure 2e

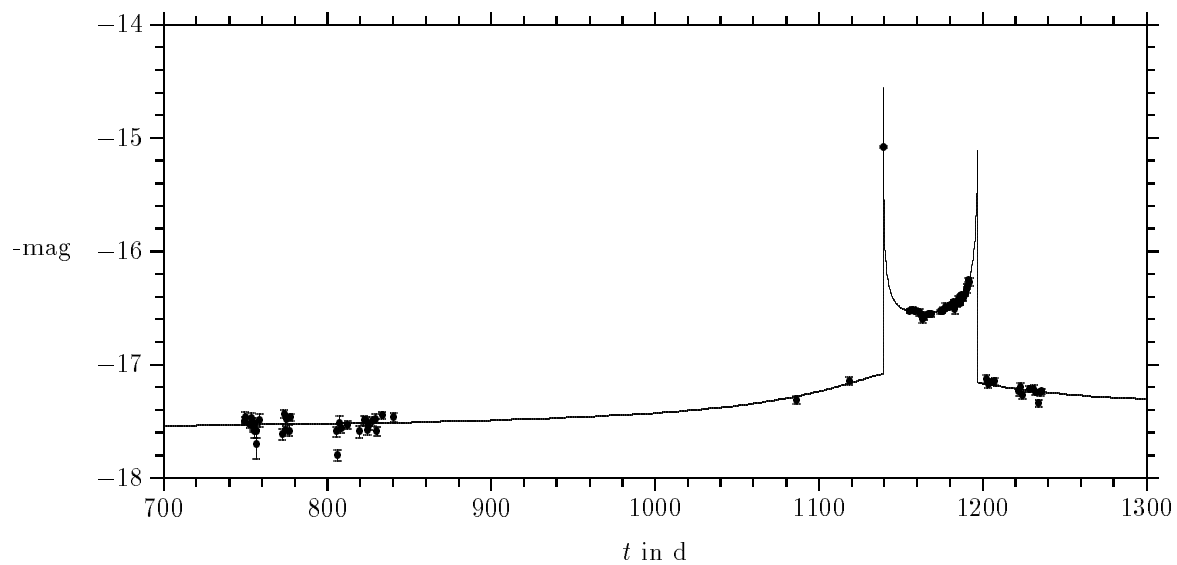


Figure 2f

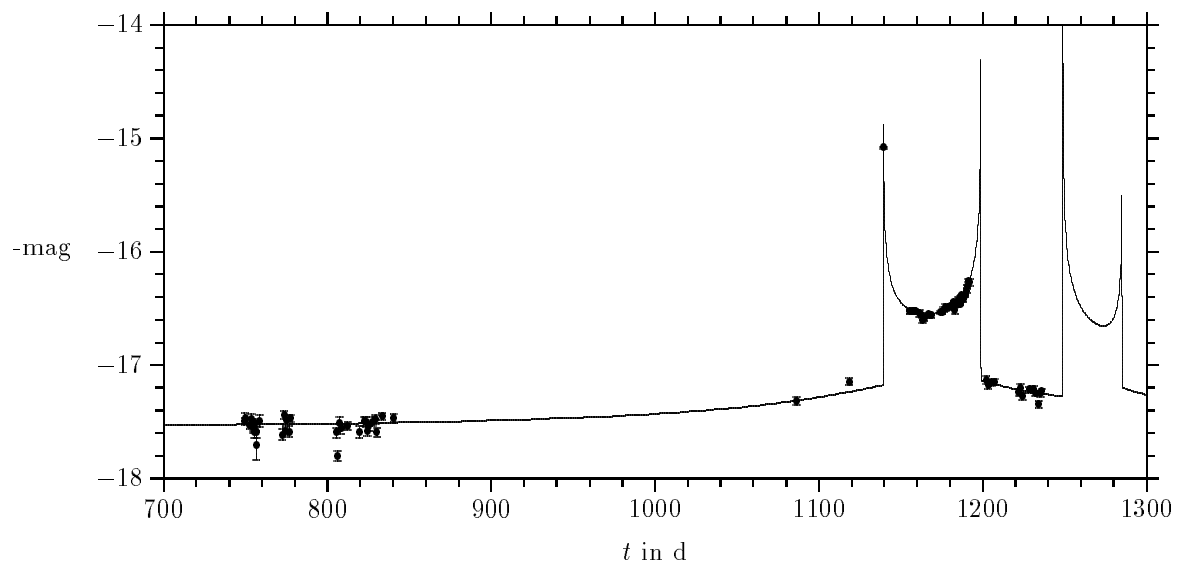


Figure 2g

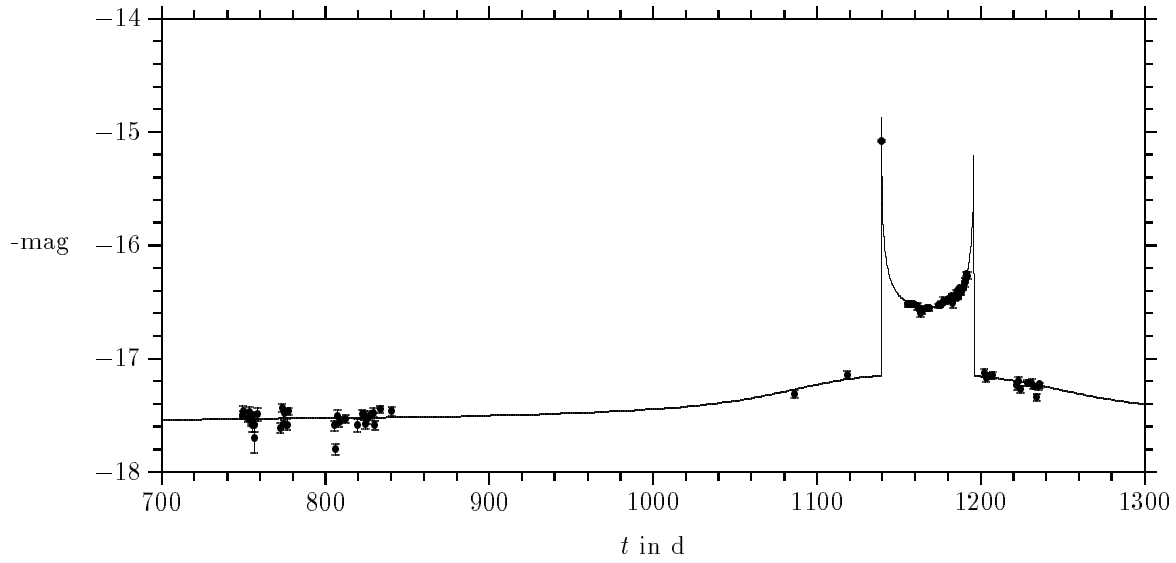


Figure 2h

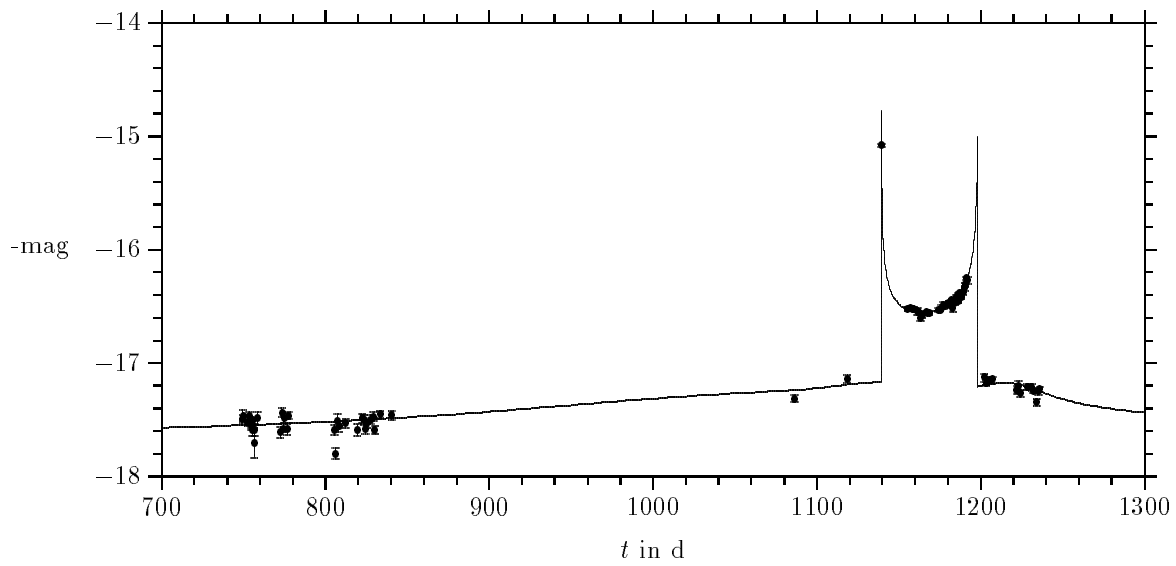


Figure 3a

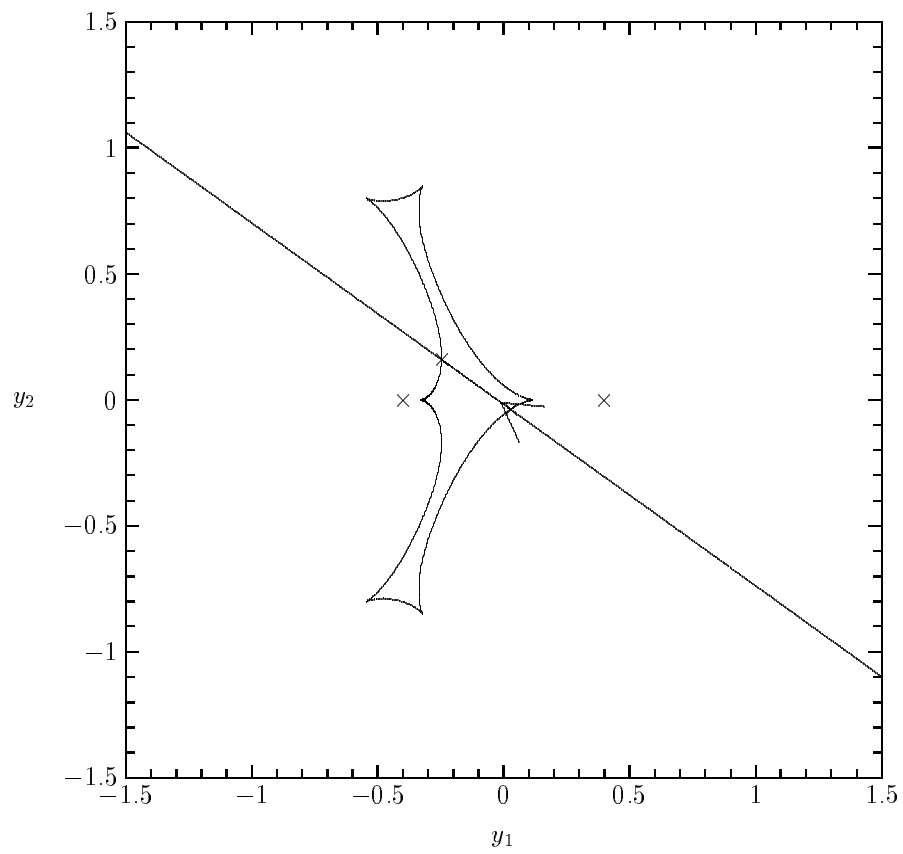


Figure 3b

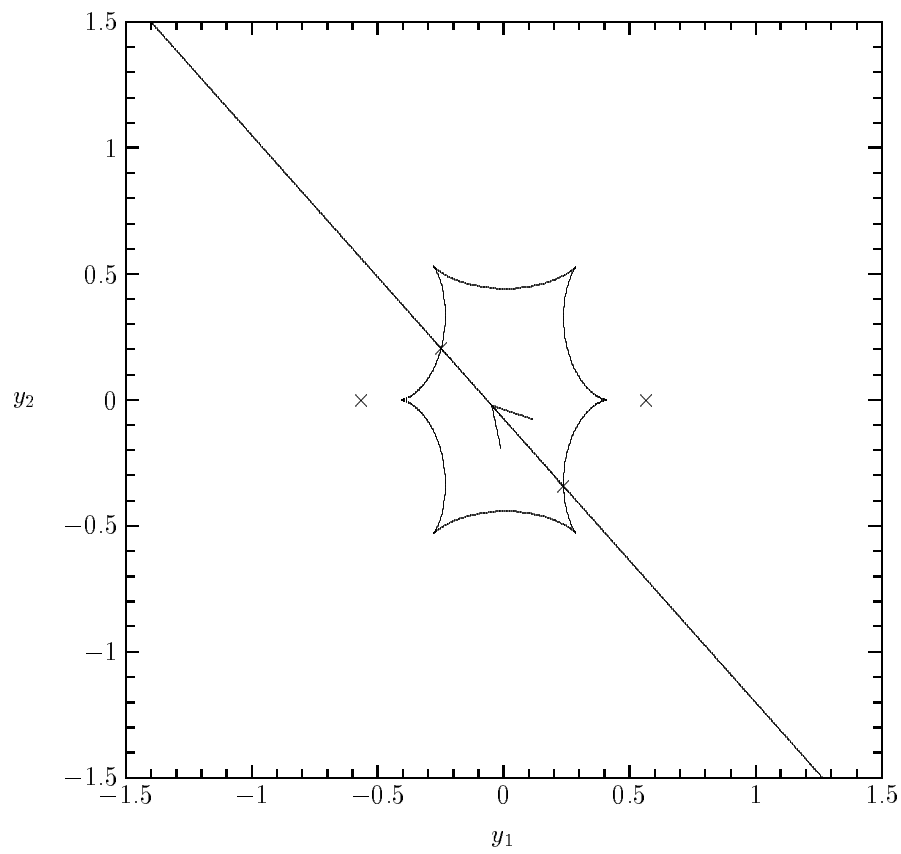


Figure 3c

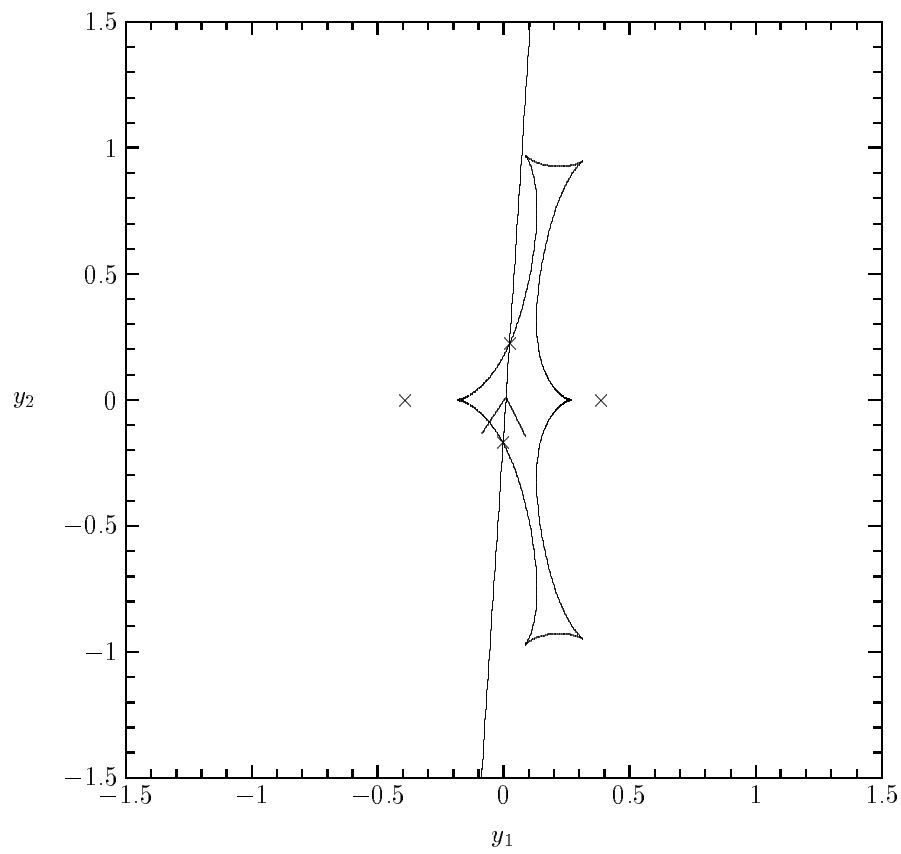


Figure 3d

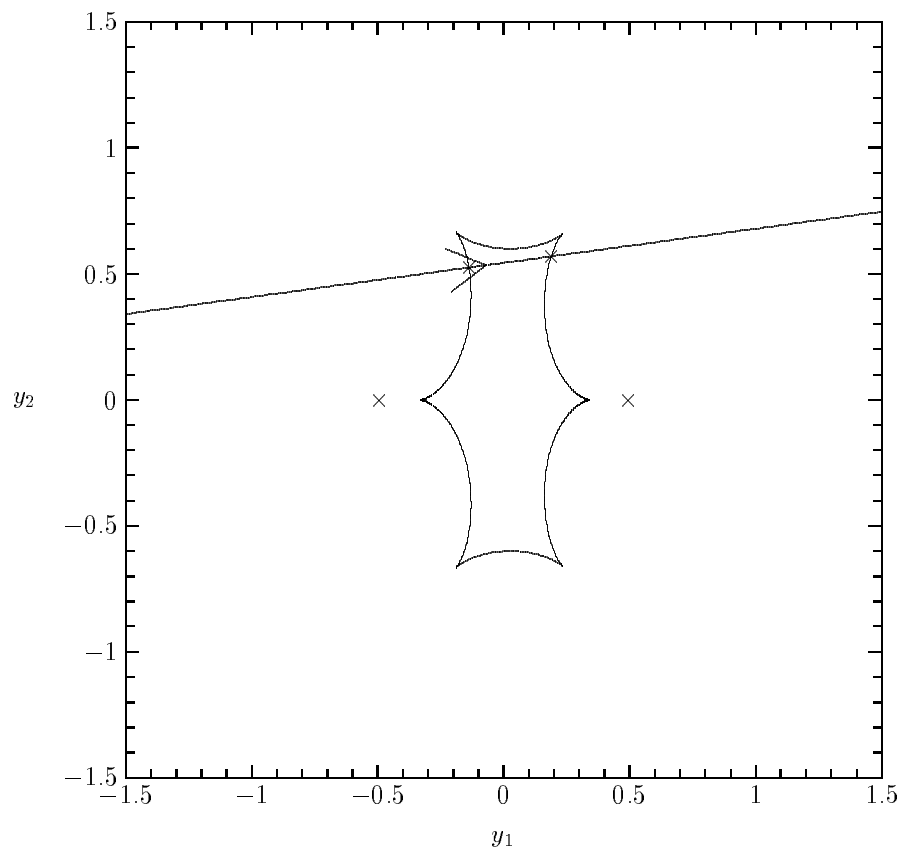


Figure 3e

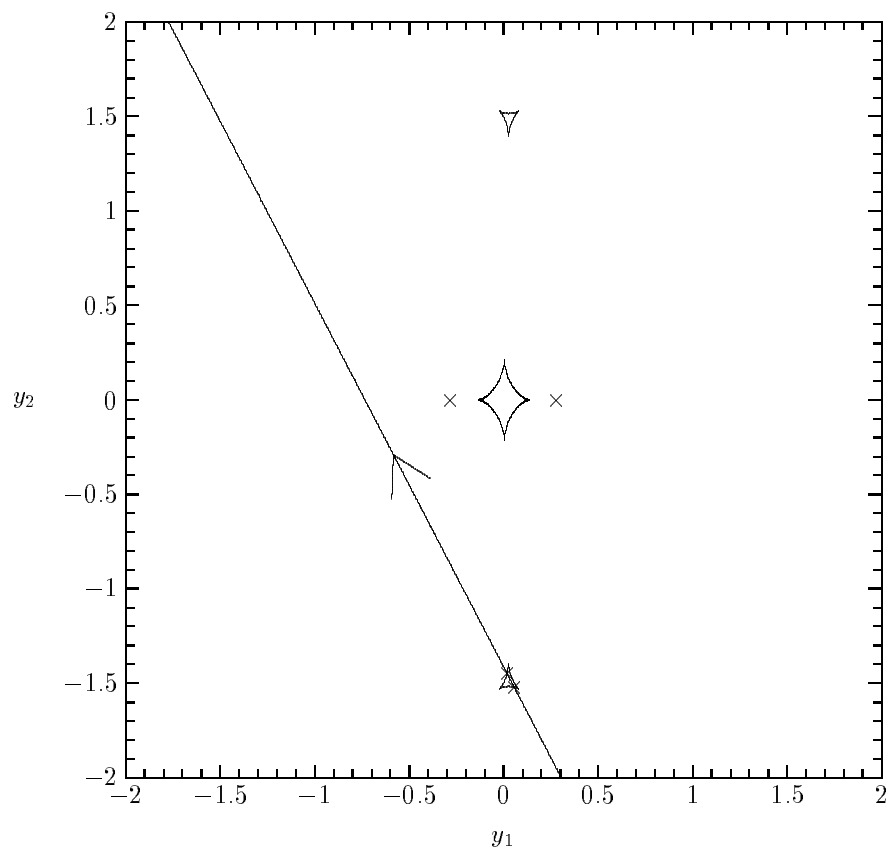


Figure 3f

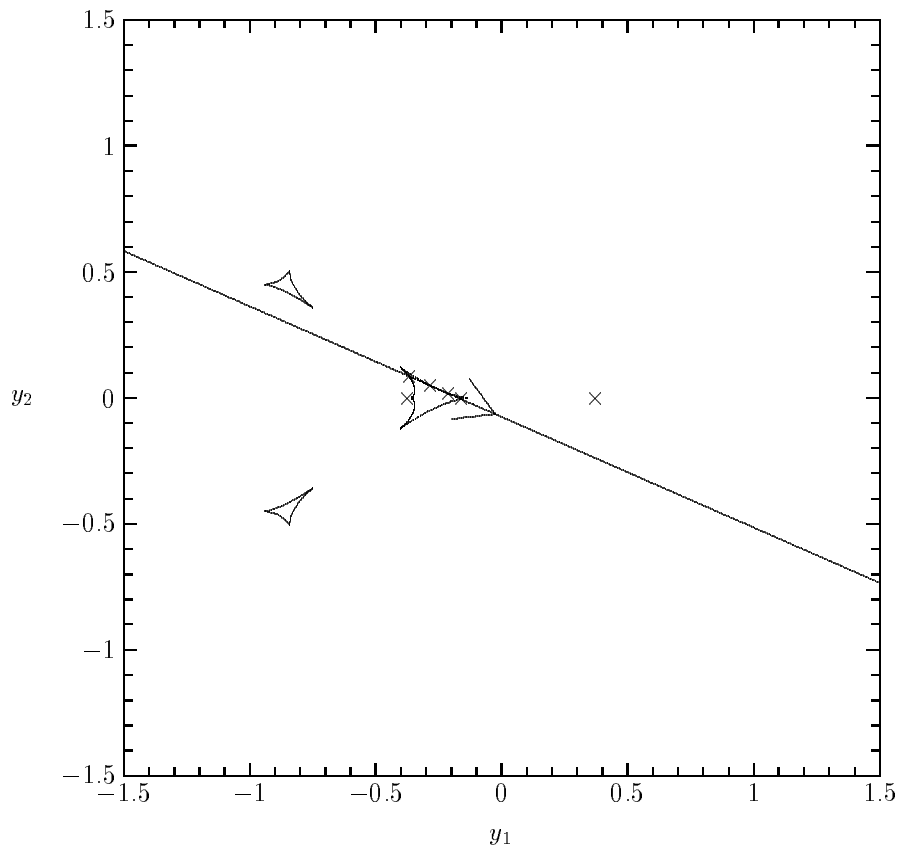


Figure 3g

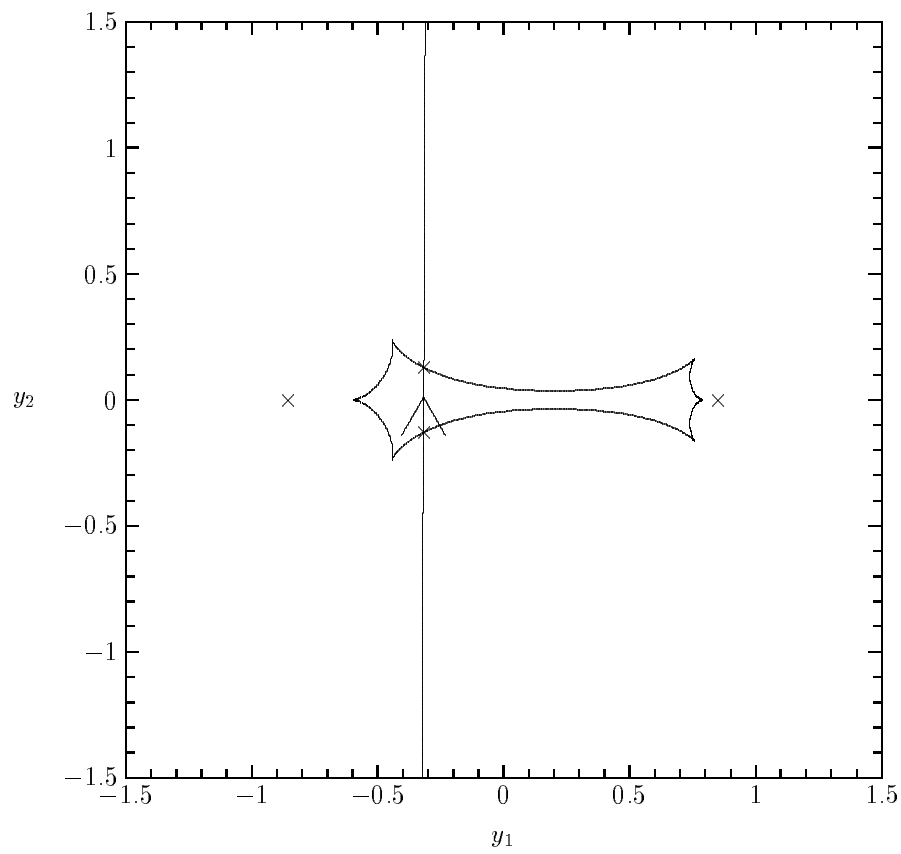


Figure 3h

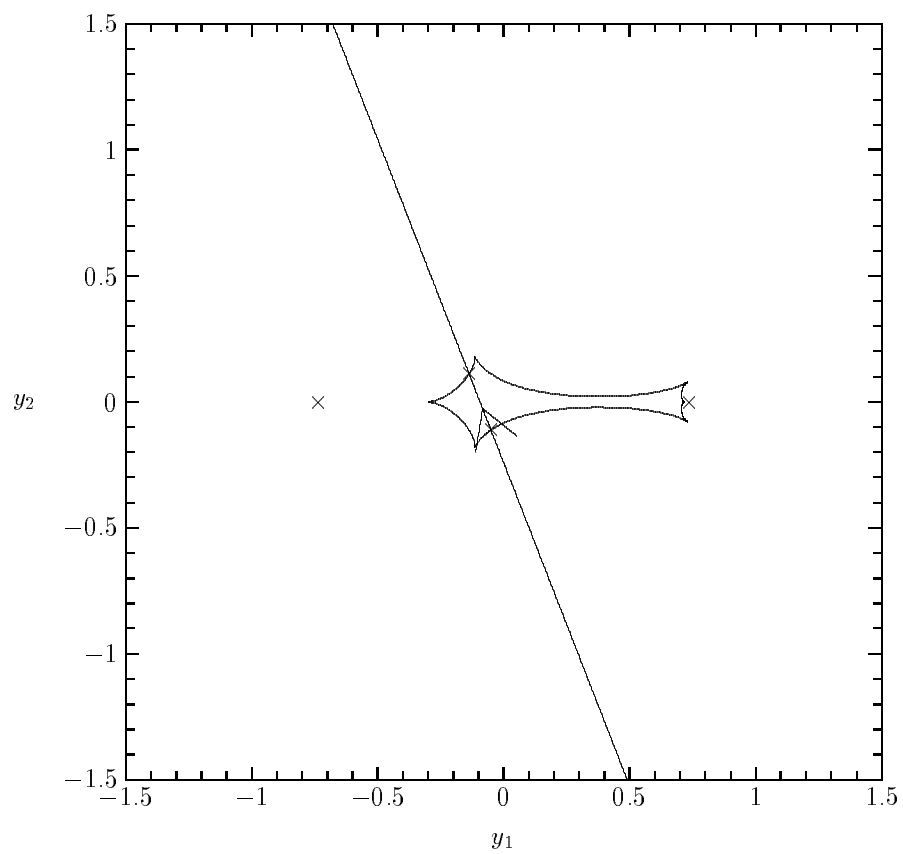


Figure 4a

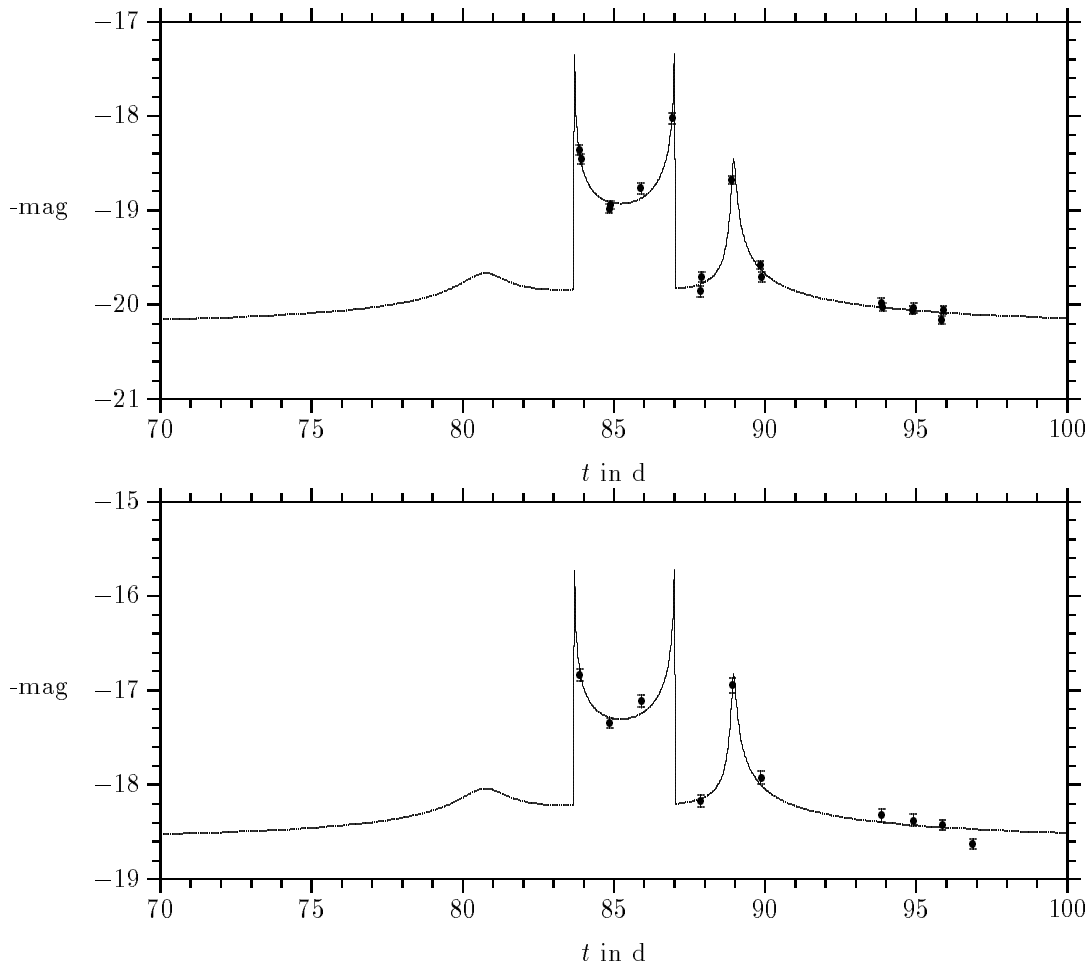


Figure 4b

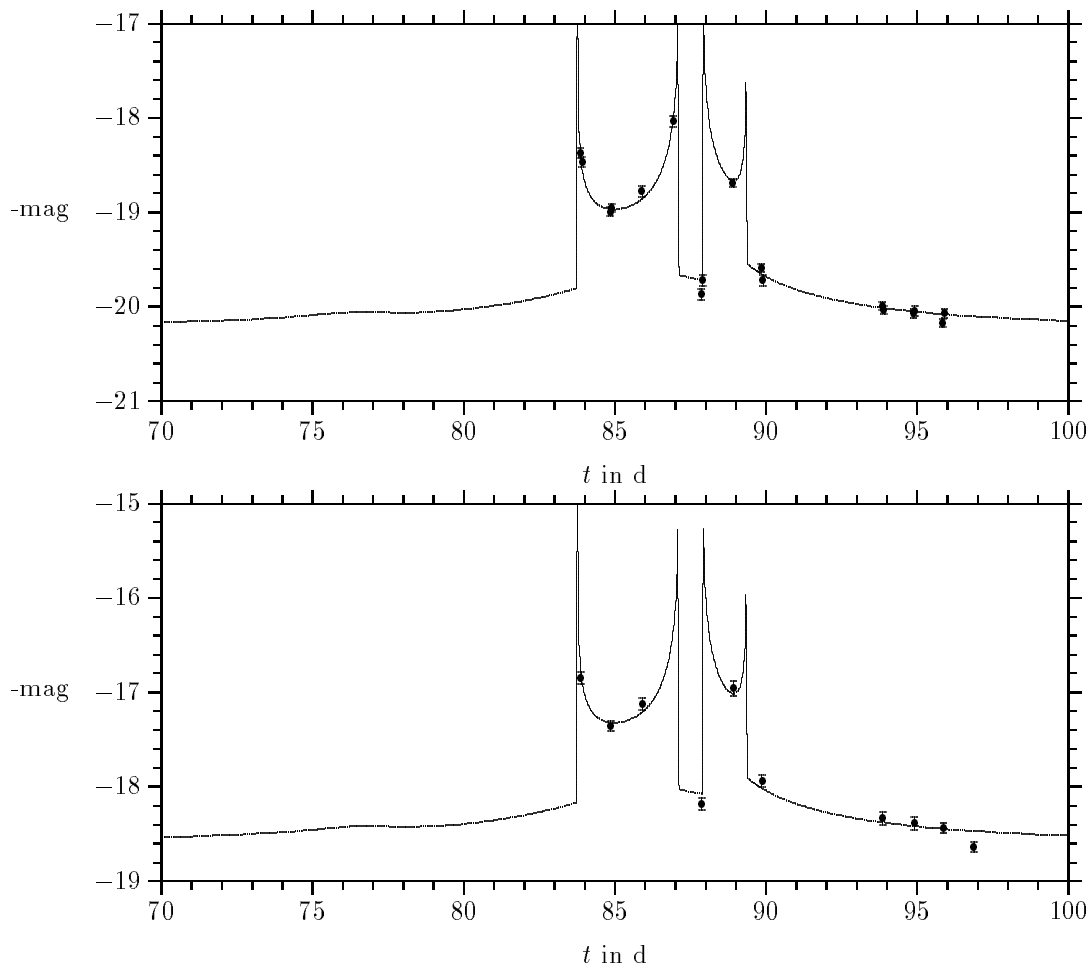


Figure 4c

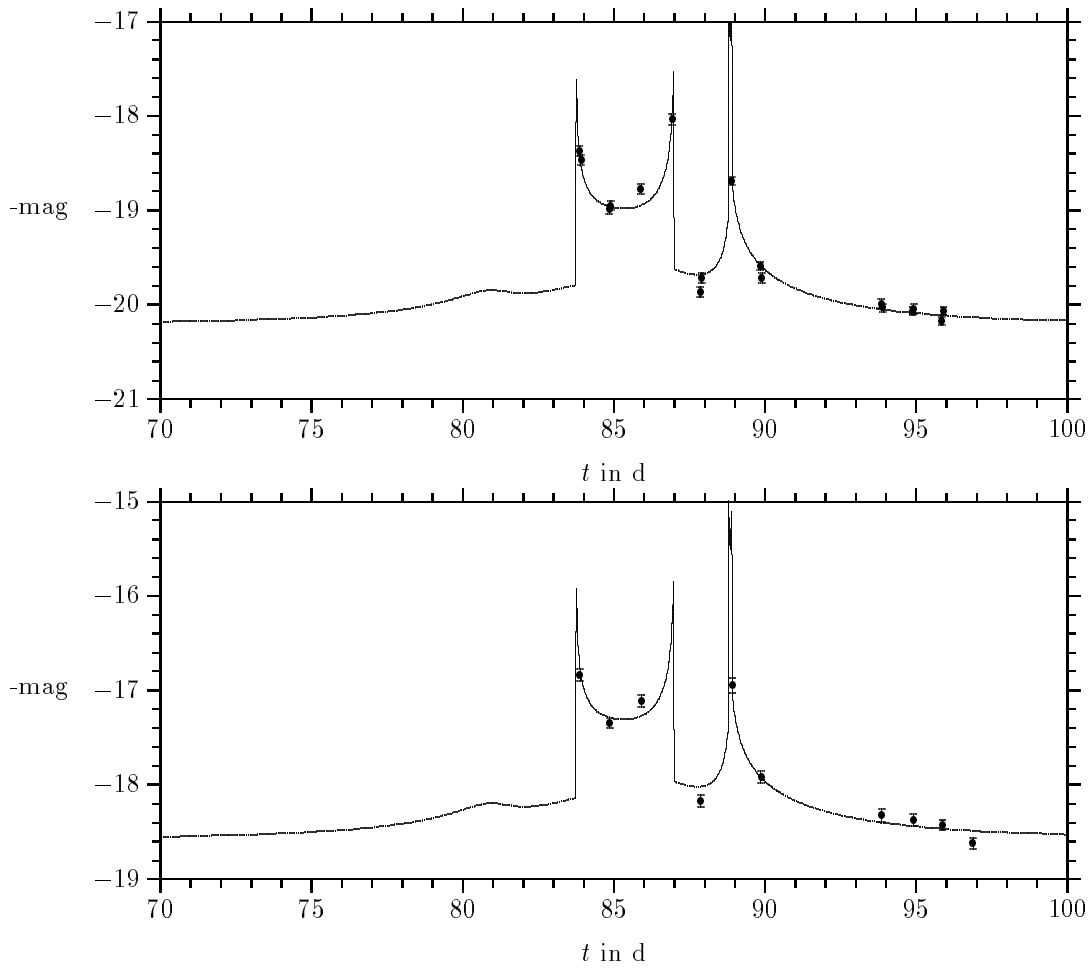


Figure 4d

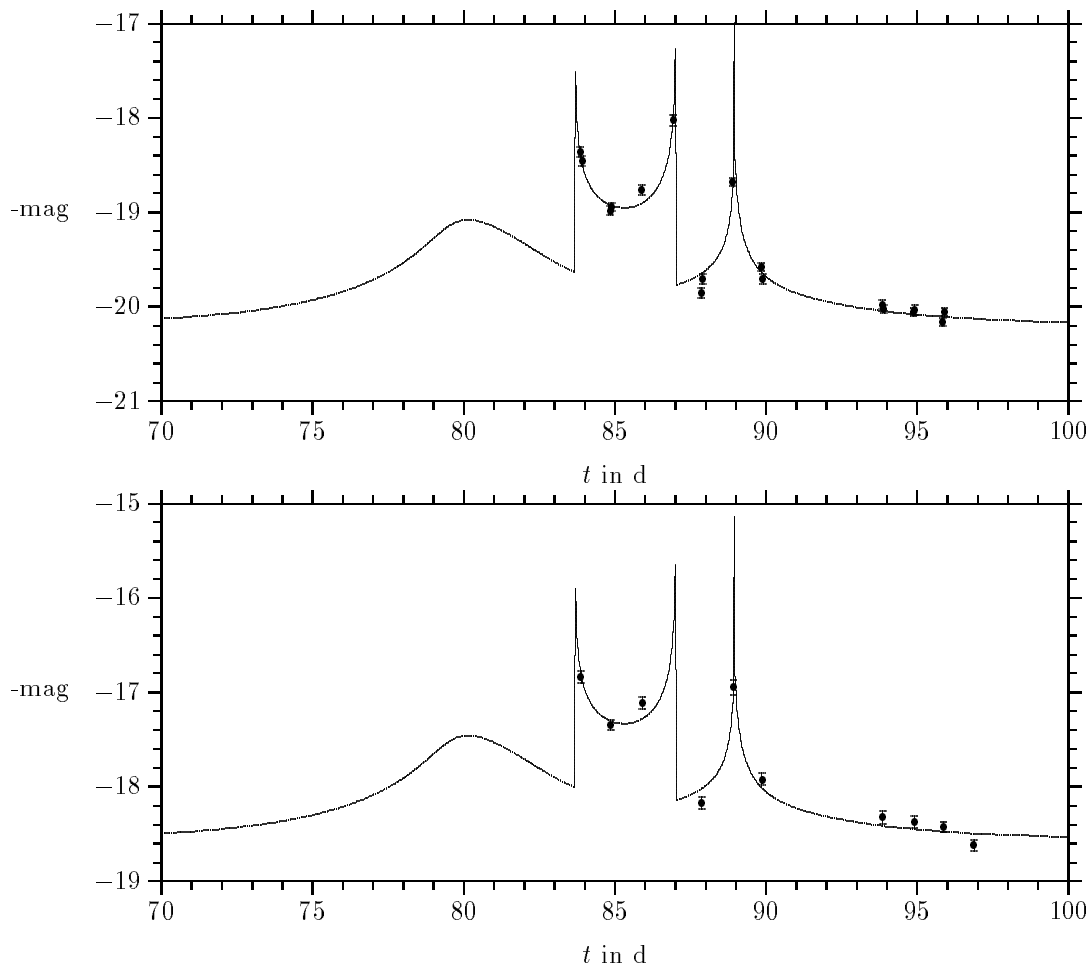


Figure 5a

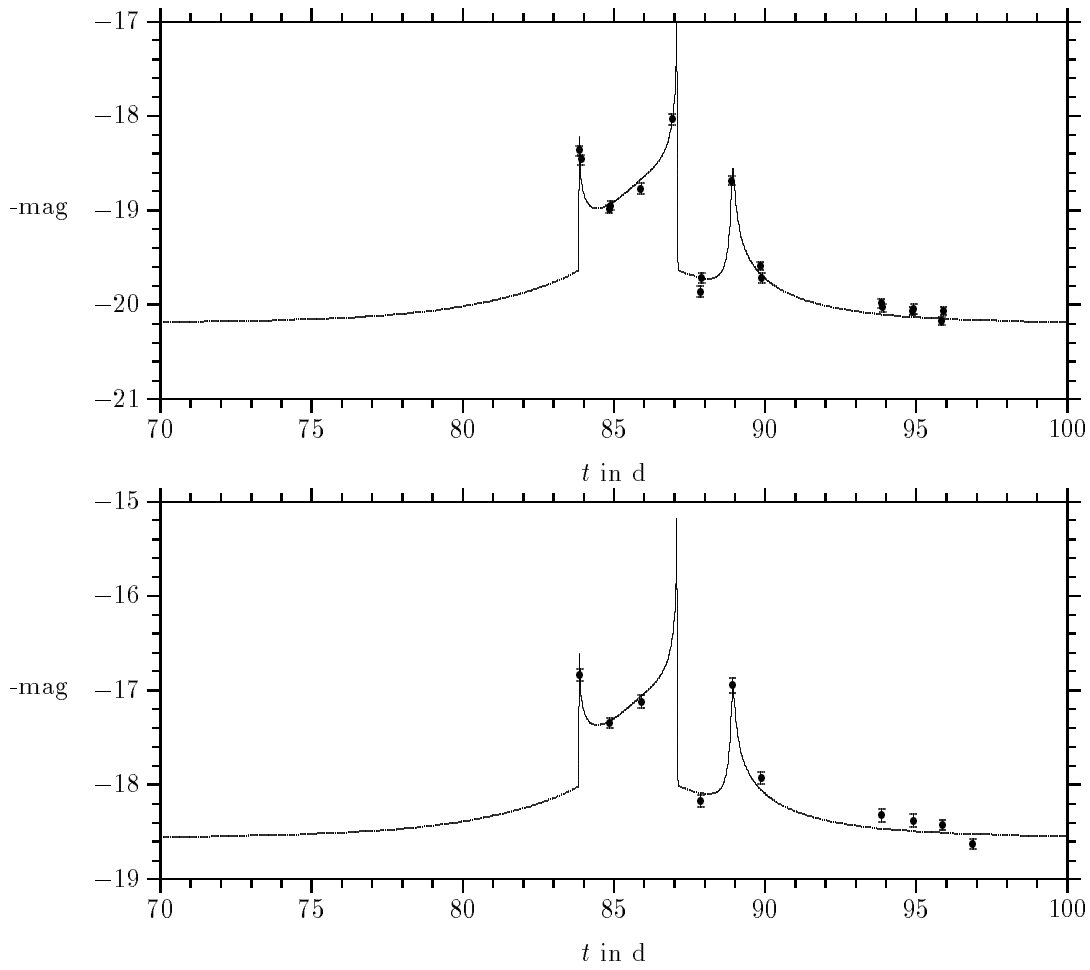


Figure 5b

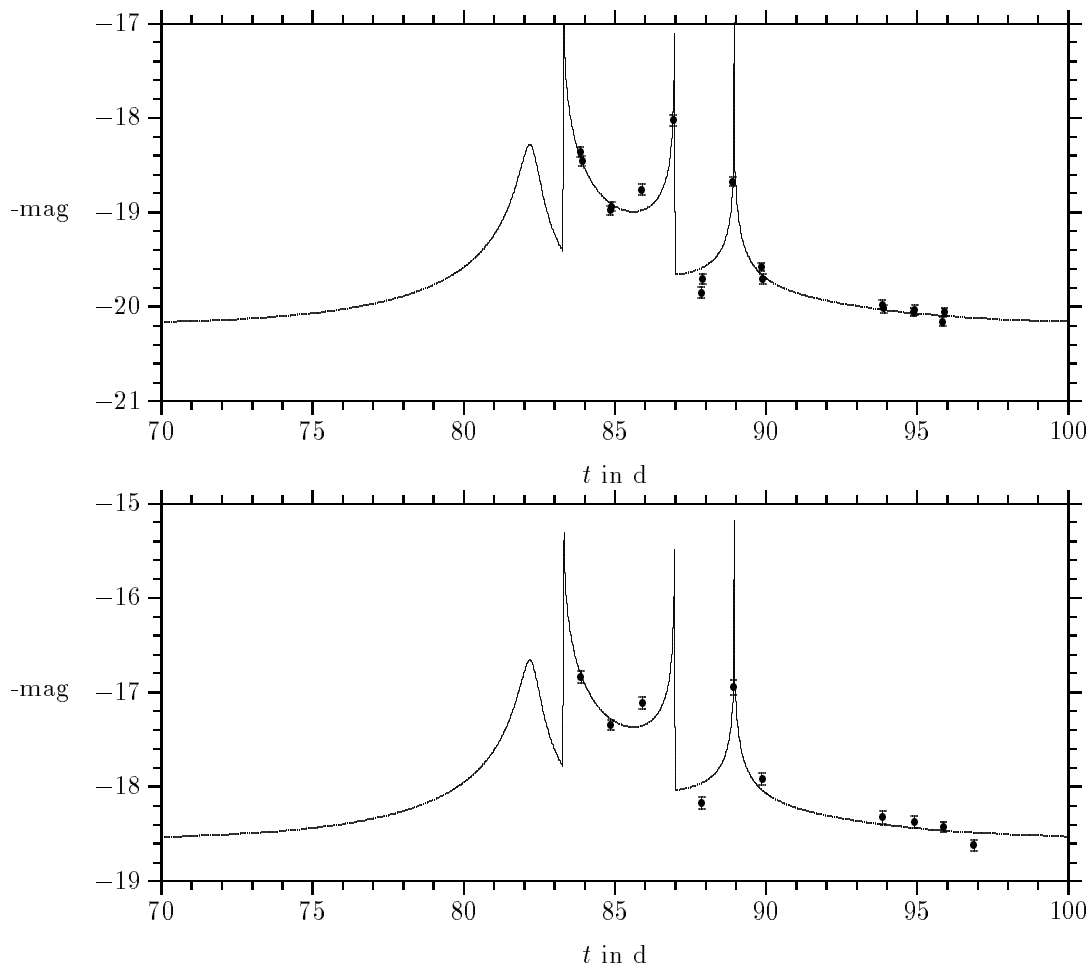


Figure 6

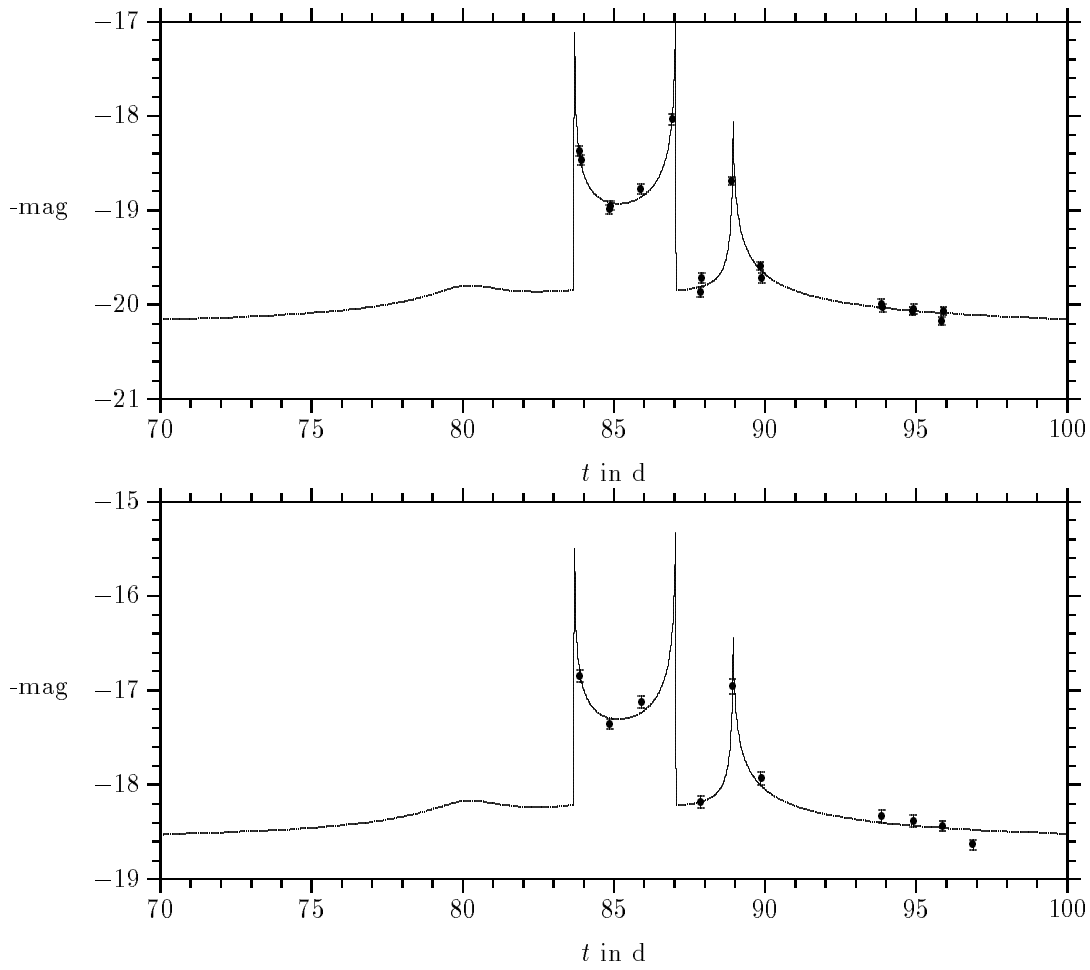


Figure 7a

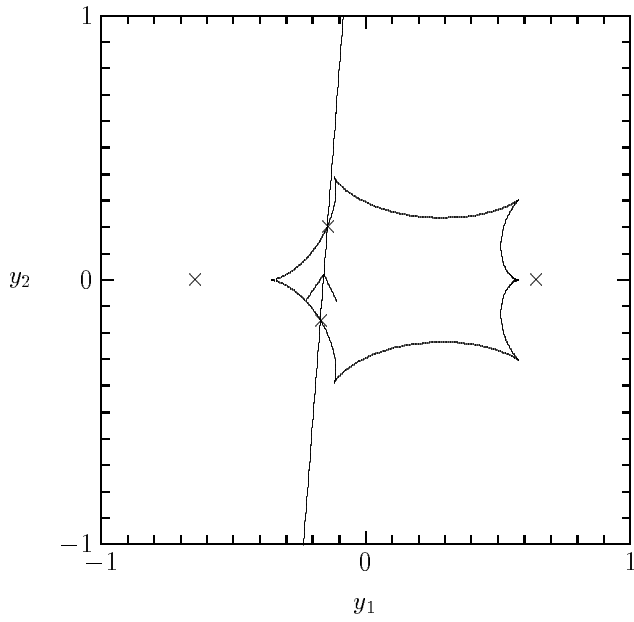


Figure 7b

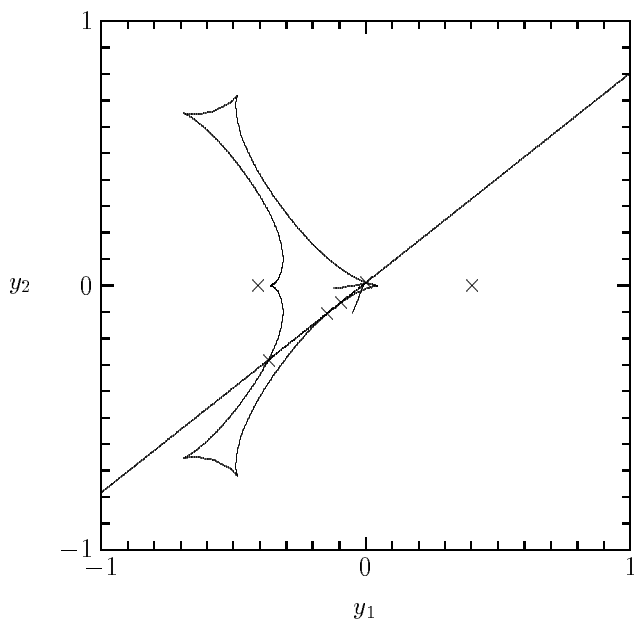


Figure 7c

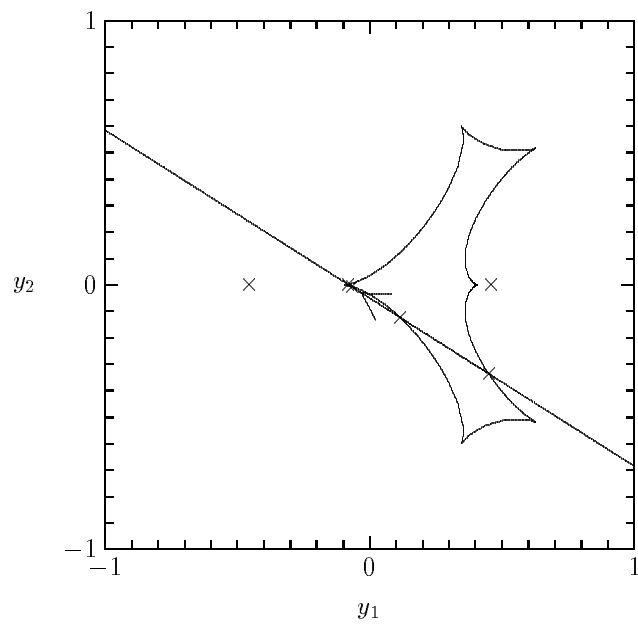


Figure 7d

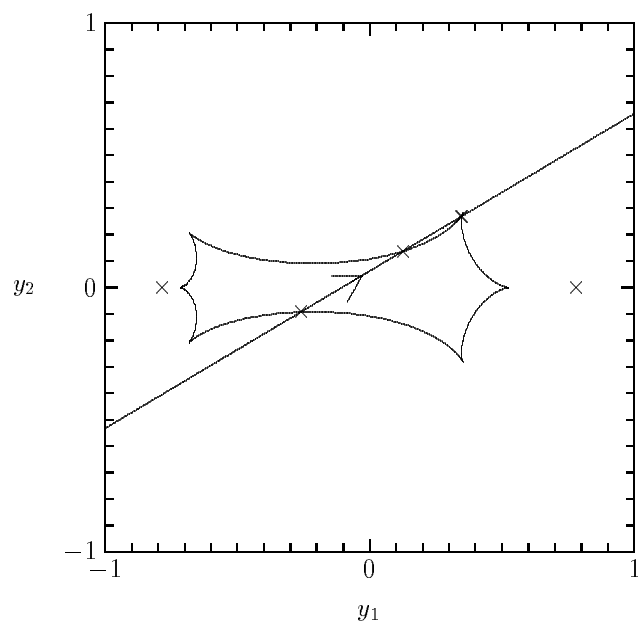


Figure 7e

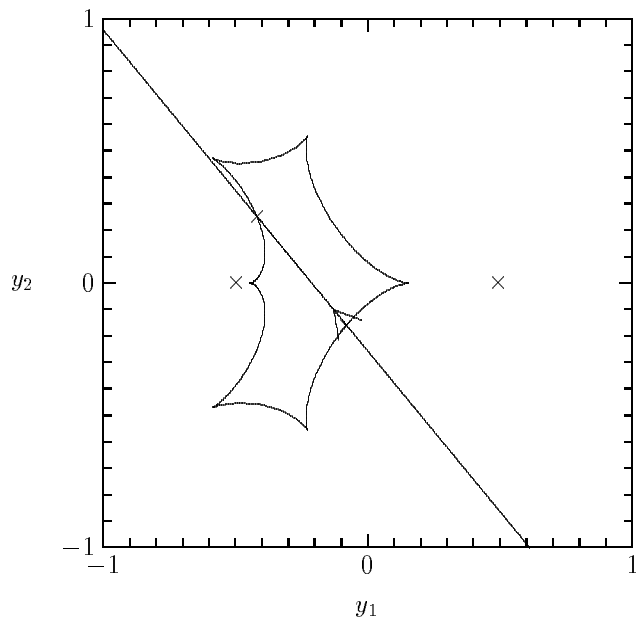


Figure 7f

